

MEMS accelerometers for mechanical vibrations analysis: a comprehensive review with applications

Marcus Varanis¹ · Anderson Silva¹ · Arthur Mereles¹ · Robson Pederiva²

Received: 7 May 2018 / Accepted: 5 October 2018 / Published online: 17 October 2018
© The Brazilian Society of Mechanical Sciences and Engineering 2018

Abstract

In this paper, the use of MEMS accelerometers for measuring mechanical vibrations is presented. Also a wide review of the literature is performed by presenting the uses of the MEMS accelerometers in a great number of applications. These sensors are known for their low prices, low power consumption and low sizes, which enhance their use in applications such as energy harvesters, monitoring processes and for educational purposes. In order to propose these sensors for measuring vibrations, a complete evaluation of the MEMS accelerometers was performed by measuring amplitudes and frequencies of oscillations and comparing their dynamic characteristics with other accelerometers with higher precision. Moreover, two experiments were conducted: In the first one, the measurements of the amplitude given by a MEMS and a standard accelerometer while being excited with sinusoidal waves with different frequencies using a vibration exciter were taken and compared. For the second experiment, three MEMS sensors and a piezoelectric accelerometer were used to measure the accelerations of a 3-DOF shear-building excited by an unbalanced DC motor. The signals obtained were compared in the time and frequency domains; for the last case, the wavelet transform, the wavelet coherence and the power spectrum density were used.

Keywords MEMS accelerometers · Mechanical vibrations measurements · Piezoelectric accelerometer

1 Introduction

Recently, there has been an increase in the use of accelerometer sensors based on microelectromechanical systems (MEMS) in engineering applications. These systems are characterized by their minimal size and low cost compared with piezoelectric accelerometers. Besides, the MEMS devices have a wide range of applications, since such systems have multiple sensing functions including temperature, pressure, acceleration and humidity sensing [1]. In addition, these devices can be used to measure not only mechanical quantities but also electrical quantities by using capacitive MEMS. It was recognized already in 1990s that this enables

important potential applications of these devices in electrical precision measurements and metrology [2].

The piezoelectric accelerometers, apart from being much more expensive than the MEMS-based ones, are not very advisable to use for low-frequency acceleration inputs due to the significant attenuation and phase shifts they exhibit when subjected to such inputs [3]. On the other hand, the MEMS accelerometers, which can be piezoresistive- or capacitive-based, are low cost and ideal for low-frequency applications. However, the capacitive-based MEMS accelerometer is less sensitive due to temperature than the piezoresistive-based, because the thermal coefficient of resistivity of doped silicon is over two orders of magnitude larger than the thermal coefficient of capacitance attained by a capacitive accelerometer [4]. In addition, in [5] a MEMS accelerometer is presented which is based on electron tunneling transducers; the accelerometer is fabricated using bulk-silicon micromachining process. These tunneling traducers have higher sensitivity than the ones based on piezoresistive, piezoelectric and capacitive accelerometers, being also smaller sized and lighter than them.

There are, in the literature, many uses of the MEMS devices also, such as energy harvesters, which are generally

Technical Editor: Wallace Moreira Bessa, D.Sc.

✉ Marcus Varanis
MarcusVaranis@ufgd.edu.br

¹ Faculty of Engineering, Federal University of Grande Dourados, Dourados, Brazil

² Faculty of Mechanical Engineering, University of Campinas (UNICAMP), Campinas, Brazil

based on piezoelectric, electromagnetic, electrostatic and hybrid mechanisms [6–12]. The mechanism most used lately for energy harvesting is the piezoelectric-based, in which strain of the piezoelectric film is converted into output voltage. The raise in the attention toward this mechanism instead of the others is mostly due to its advantages of high conversion efficiency and easy implementation [13–15]. Although the piezoelectric-based has several advantages comparing to other mechanisms, the potential to scale down to much smaller sizes is greater for electrostatic converters [16]. Also, with electrostatic converters a close integration with electronics can be achieved through MEMS processing technology, which can be a challenging task for piezoelectric converters. For a recent application, in [17] a rainfall energy harvester is presented, where the measuring system consists of MEMS piezoelectric accelerometers and an Arduino. In addition, as the device used for energy harvester will have a maximum electrical power generated at its resonance frequency, the knowledge of the value of it is very important. The methods to measure the frequency range from blur-envelope techniques [18] and viscous damped measurements [19] to sophisticated electronic measurements [20]. Also, in [21] an harmonic distortion technique is proposed to measure the resonance frequency, which also provides the damping factor of the system through the determination of the filter parameters as the cutoff frequency, and in [22] a MEMS accelerometer is characterized by means of computational and optoelectromechanical methodologies.

The small size of MEMS devices also motivates its use in some monitoring processes such as the Structural Health Monitoring (SHM) [23–26], the Machine Condition Monitoring [27–29], damage detection [30] and for navigation systems such as strap-down Attitude and Heading Reference Systems (AHRS) and Inertial navigation system (INS) [31]. For some examples, in [32] a MEMS accelerometer is designed for SHM applications, where sensing low frequency and low amplitudes with good resolution is essential; in [33], a computer-aided analysis of three bulk micromachined piezoresistive MEMS accelerometer is made for concrete SHM applications, where three accelerometers have different design characteristics. Although the MEMS accelerometers have high potential in monitoring processes, there is little existence of such sensors for SHM in the present sensor market as pointed out in [32]. It is worth noting, however, that the accuracy and the lifespan of sensor boards installing accelerometers and multiple sensors are lower than dedicated boards on the market focused on SHM. In addition, the MEMS accelerometers have possible applications in navigation systems such as AHRS due to their characteristics already cited of small size, lightweight, low power and low cost. However, these sensors introduce great errors that must be compensated in order to make use of them in navigation systems. Examples are shown in reference [34]

where the results of an AHRS having low-cost MEMS-based in a three-axis flight turntable are shown and validated in a practical application where the system was mounted in a micro-Unmanned Aerial Vehicle (UAV), and the errors due to gyroscopic drift are detected and corrected by a multi-sensor data fusion algorithm that uses benchmark reference vectors. Another application is presented in [35] where a MEMS-based rotary strap-down inertial navigation systems is developed, in which the significant sensor bias is automatically compensated by rotating the inertial measurement unit.

Implementation of the MEMS devices combined with a wireless technology in wireless sensor networks (WSNs) is widely researched in the literature from monitoring processes to energy harvesters [36–49]. This technology has the benefit of avoiding some problems and limitations that one may face due to the use of wired networks. Besides, the MEMS devices are characterized by their low cost and power consumption, which are valuable characteristics for wireless sensors or wireless sensor networks. However, there are still some problems in the WSNs regarding the sampling rate and the synchronous acquisition, which are essential for a wireless network. These problems are solved in references [50] and [51], where WSNs are designed and developed for machine vibration monitoring and SHM, respectively; also, both papers tested the networks experimentally by improving some features of traditional WSNs that allowed the system to have a improved sampling rate and a good synchronous acquisition. In addition, reference [52] presents a FPGA-based wireless sensor nodes for vibration monitoring and fault diagnosis for rotating machinery, where experimental tests were conducted in a rotating machine with an unbalance fault.

Furthermore, in some applications, the MEMS devices are used together with the Arduino microcontroller as an acquisition system in the wireless sensor nodes [53–58]. This use brings a lot of benefits, but one may emphasize the low cost and easy implementation. For such reasons, the Arduino has been used as an acquisition system for educational purposes [59–68]. In [69], the MEMS technology is applied to high school classes with the purpose of increasing the interest to the students in natural sciences and engineering to fill the lack of qualified personnel. Some other applications of the Arduino are presented in [70], where the control of a small wind turbine is shown with the use of the Arduino and in [71], where a brushless DC motor is designed to incorporate a hybrid electric vehicles, and the Arduino is used to acquire the experimental data. In addition, the new developments in open-source hardware/software, standardization and commercialization of wireless sensor network technologies have helped to reduce the complexity of implementing wireless sensing and actuation systems and have made it fairly easy to implement a

prototype system for proof of concept and demonstration purposes [72].

Taking into account all the aforementioned uses of MEMS devices in a great number of applications, it is very important that the limitations of such devices are known. In that sense, this paper presents the evaluation of three MEMS accelerometers as mechanical vibration sensors. For such purpose, two experiments were performed: In the first one the measurements with a ADXL-335 sensor and a standard accelerometer were taken by using a vibration exciter for further comparison of the signals. The results showed that it is not advisable to use the MEMS accelerometer for evaluation to measure amplitudes in applications with high frequencies, since the uncertainties associated with the measurements increased with the raise of the frequency of excitation. However, it was concluded that the accelerometer evaluated can be used for low-frequency applications with a considerable reliability.

In the second experiment, the MPU-6050, the ADXL-345, and the ADXL-335 were used to measure the acceleration of a 3-DOF shear-building structure. In order to evaluate these MEMS sensors, the signals were compared in the time and frequency domains with an accelerometer with higher precision. The results showed that the sensors can be used in low-frequency applications. In addition, to perform the signal acquisition of the MEMS accelerometers, the Arduino microcontroller was used, which is a low-cost alternative that gives good results. In addition, the main contribution of this paper is the validation of MEMS-based accelerometers for mechanical vibration analysis, more specifically, in applications where the frequency and the amplitude need to be measured.

This paper is divided into five sections: In Sect. 2 the description of the MEMS accelerometers is presented, while in Sect. 3 the experimental procedures are shown for both experiments: the calibration of the ADXL-335 and the evaluation of the other accelerometers. The other Sects. 4 and 5 present a discussion of the results obtained and the final comments of the paper, respectively.

2 MEMS accelerometers

The MEMS-type accelerometers are often divided into piezoresistive- and capacitive-based accelerometers. The piezoresistive accelerometers measure acceleration based on the oscillations of a beam which has a proof mass mounted at its end. A piezoresistive element is also mounted on the beam at a known position; the oscillation of the beam changes the resistance of the patch which generates an electrical signal that is proportional to the acceleration of the vibration that the sensor is subjected. On the other hand, the capacitive-based MEMS accelerometers measure the acceleration

through the changes of the capacitance between a proof mass and a fixed conductive electrode separated by a narrow gap [73]. In order to compensate the drifts and interferences as well as to linearize the deflections that the sensor may be subjected to, differential capacitors are employed. However, the capacitive-based accelerometer, as well as the piezoresistive-based, still show some deviations in amplitude and phase. In [74], a filter is designed to improve the signals measured with the MEMS accelerometers through the calculation of a characteristic function (which is the inverse of the frequency response function) with reference to a standard accelerometer, which corrects the amplitude and phase deviation; in [75] a solution for the problem of determination of errors generated by systems measuring dynamically changeable signals is proposed by means of the signals maximizing chosen error criterion.

The capacitive MEMS-based accelerometers stand out from the piezoresistive-based due to the less temperature variation, because the latter are more sensitive to thermal excitation than the former, since the viscosity of the damping fluid used to eliminate resonant amplification and extend over-range capability is a strong function of temperature in the piezoresistive accelerometers [76, 77]. Since the gaseous dielectric capacitors are relatively insensitive to temperature variations, capacitance sensing provides a wider temperature range of operation, without compensation, than piezoresistive sensing [4]. Also, besides the superior measure capacity of the capacitive accelerometers, they are often chosen rather than the piezoresistive ones because their costs have been dropping due to the reduced fabrication costs. Problems with temperature coefficients of the piezoresistive materials embedded in the sensors have required additional design features, which increased their price [78].

However, despite the disadvantages aforementioned about the piezoresistive accelerometers, their use is still motivated, since they have a low-noise property at high frequencies when compared to capacitive accelerometers. In addition, the costs of the piezoresistive sensors can now be reduced by new manufacturing processes such as deep ion etching (DRIE) techniques [78]. An important application of these types of sensors is in the identification of damage in structures, where the use of high-frequency local response measurements is presented to be successful [79]. Therefore, in these cases the piezoresistive accelerometers are more suitable than the capacitive ones.

2.1 ADXL-335 accelerometer

One of the MEMS accelerometers that will be evaluated in this paper is the ADXL-335 from Analog Devices, which is shown in Fig. 1a. Different from the other accelerometers evaluated, the ADXL-335 is an analog sensor. This accelerometer is characterized by its small size and low power

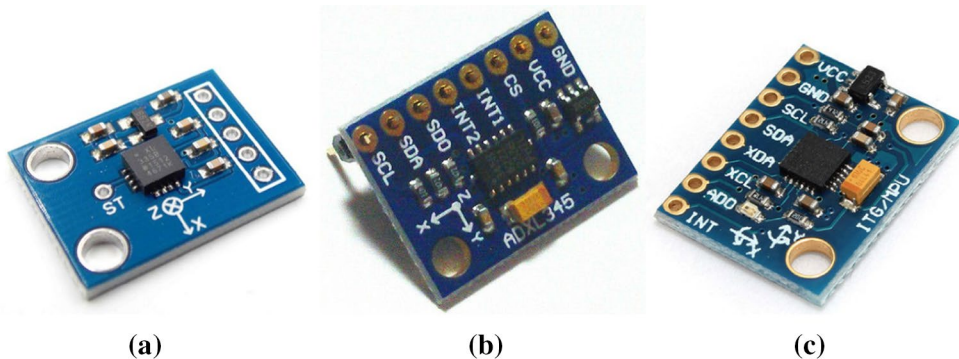


Fig. 1 Accelerometers used: **a** ADXL-335, **b** ADXL-345 and **c** MPU-6050

consumption and has the ability to measure acceleration in the three axes in a range of ± 3 g with a signal conditioning voltage output [80]. The ADXL series MEMS accelerometers use a comb finger-type differential capacitive MEMS structure and have excellent sensitivity, low drift, good noise performance and simplicity [81–83]. The sensor measures vibrations due the capacitance variation in differential capacitors, and it can be used to measure the static acceleration of gravity and accelerations due to motion, shock or vibration. Also, the accelerometer has a very low temperature hysteresis, commonly less than 3 mg in the temperature range from -25 to 70 °C. In addition, the ADXL-335 requires a voltage input from 1.8 to 3.6 V, and it has a typical consume of 350 μ A.

Due to the very small size of the accelerometer, 4 mm \times 4 mm \times 1.45 mm, the ADXL-335 is commonly mounted in a breakout board for easy handling. In this work, the GY-61 breakout board model was used, which has dimensions of 21 mm \times 15.5 mm \times 3 mm. The board used has also a voltage regulator model 662K, which regulates the input voltage, powering the accelerometer with a constant voltage of 3.3 V, that promotes a better quality of the measured signals. In this work, the Arduino was used as a acquisition system; thus, the signal from the ADXL-335 is digitalized by the analog-to-digital converter (ADC) of the Arduino. Further, capacitors are embedded in the board for the purpose of improving the measurement resolution and for preventing aliasing.

As the ADXL-335 accelerometer is of small size, it can be used in a wide range of applications, from electronic devices and interfaces with the purpose of controlling unmanned aerial vehicles (UAVs) to engineering applications such as in geoengineering [84] or in Machine Health Monitoring [85]. Since the accelerometer has a little temperature hysteresis, it turns to be a great device for monitoring structures that suffer from significant temperature variation, as, for example, structures located in sites subjected to snow weather or in desert-like places. For more applications, in [86] two-axis

MEMS-based accelerometers were used for near-surface monitoring of geotechnical systems, in [87] a self-power vibration measurement system is proposed which is based on a piezoelectric material which harvests the energy from ambient vibration source and transforms into useful electrical output power of a ADXL-335 accelerometer, in [88] a wireless and battery-free passive sensing platform is proposed for structural damage detection; in [89] bridge health monitoring system is suggested; in [90] a current transducer is used for monitoring of supply current for detection of bearing fault.

2.2 ADXL-345 sensor

The ADXL-345 sensor of Analog Devices is a MEMS three-axis accelerometer with dimensions of 3 mm \times 5 mm \times 1 mm and is shown in Fig. 1b. Just like the ADXL-335 sensor, its functioning mechanism is based on the variation of the capacitance in differential capacitors, which allows the sensor to measure static and dynamic accelerations in a range up to ± 16 g. In the ADXL-345, before the acceleration data are sent to the signal acquisition by means of the I2C and SPI protocols, the data pass through a 13-bit ADC. Also, the range of the measurements is user-programmable between the options: ± 2 , ± 4 , ± 8 and ± 16 g. Besides, the variation of the sensitivity of the sensor due to temperature is ± 0.01 %, and the sample frequency can be chosen from 0.1 Hz to 3.2 kHz.

As the sensor is of small sized and has to be powered with a voltage between 2 and 3.6 V, it was mounted in a breakout board model GY-291 of dimensions 20 mm \times 10 mm, which has a voltage regulator model KB33 that allows the board to be powered with a 5 V. In order to allow the board to be mounted in a surface, it has two holes with diameters of 3 mm.

This accelerometer has a wide range of application, for some examples: in [91] they focus on characterizing the kinetic energy that can be harvested by a wireless node

with an Internet of Things form factor and on developing energy allocation algorithms for such nodes; in [92] an application, design and implementation of a novel vibration-powered sensing system for condition monitoring of engines is presented; in [93], a self-powered smart tag for wireless SHM in aeronautical applications is presented; reference [94] presents in detecting induction motor faults caused due to electrical or mechanical origin by vibration analysis; and in [95] a machine tool vibration fault monitoring system based on Internet of Things is studied and established.

2.3 MPU-6050 sensor

The MPU-6050 chip of Invensense is a device that integrates a three-axis accelerometer and gyroscopic sensors in a $4\text{ mm} \times 4\text{ mm} \times 0.9\text{ mm}$. The functioning of the accelerometer of the MPU-6050 is identical to the other accelerometers presented above, and the gyroscope measures the angular velocity due to the Coriolis effect which causes a vibration that is detected by a capacitive pickoff. In addition, the max sampling frequency of the accelerometer and the gyroscope is 1 kHz and 8 kHz, respectively. Also, the MPU-6050 has three 16-bit ADCs for digitizing the gyroscope outputs and three 16-bit ADCs for digitizing the accelerometer outputs. Figure 1c shows the MPU-5060 accelerometer.

As the chip of the MPU-6050 is very small size and has to be powered in a voltage between 2.375 and 3.46 V, it is mounted in a breakout board, in this case a GY-521 of dimensions $20\text{ mm} \times 16\text{ mm}$, which has a voltage regulator model KB33 just as the others breakout board described above, that allows the board to be powered with a voltage up to 5 V.

Although the accelerometer sensor of the MPU-6050 has a maximum range of measurements of $\pm 16\text{ g}$, the range is also user-programmable in the ranges of $\pm 2, \pm 4, \pm 8\text{ g}$. The sensor has a little variation in the sensitivity due to temperature which is of about $0.02\text{ }^{\circ}\text{C}$. On the other hand, the gyroscope sensor has a maximum range of $\pm 2000\text{ }^{\circ}/\text{s}$, and its variation on the sensitivity due to temperature is $\pm 2\%$. Only the accelerometer sensor will be evaluated in this paper.

The MPU-5060 can be used in many applications; for example, reference [96] presents a solution on how to generate a power for marine wireless sensors using underwater motion energy; in [97] a damage detection method is made based on autoregressive model (AR) and damage-sensitive features (DSFs); reference [98] proposes the development of a sensing system that uses the Arduino platform and a MPU-5060 accelerometer; and in [99] two compact and portable motion sensing systems to

monitor the dynamic behavior of complicated structures are presented.

3 Experimental setup

The objective of this paper is to perform a calibration of the accelerometer ADXL-335 and an evaluation of it and two other MEMS accelerometers: the ADXL-345 and the MPU-6050. Therefore, two experiments were carried out: the first one presents the calibration of ADXL-335 by comparing its given signals with a standard accelerometer using a vibration exciter, and in the second experiment a comparison was made with the measurements given by the MEMS accelerometers and a sensor with higher precision in a 3-DOF shear building excited by an unbalanced DC motor.

3.1 Experiment 1: calibration of the ADXL335 accelerometer

The experimental apparatus used for calibrating the ADXL-335 accelerometer is composed of a Vibration Exciter (shaker) Type 4809 of Brüel and Kjær, a Programmable X-tal controlled function generator Type TR-0467 of Elektronikus Mérökészülékek Gyára (EMG), a Power Amplifier Type 2706 of Brüel and Kjær, a Spectral Dynamics SD380 Signal Analyser of Scientific-Atlanta and a standard accelerometer model 2270 of Endevco.

The standard accelerometer used has crystal Piezite® Type P-10 which provides a high performance for the

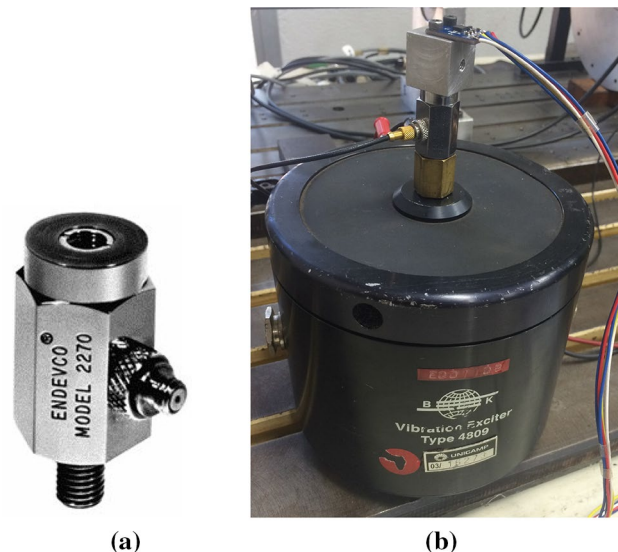


Fig. 2 **a** Standard accelerometer Endevco model 2270 and **b** experimental setup

calibration of other sensors. The frequency and amplitude range for calibration with this accelerometer is from 5 Hz to 10 kHz and from 0.2 to 10,000 g, respectively. In addition, the standard accelerometer was previously calibrated and its sensitivity is 1000 mV/g. Figure 2a shows the accelerometer used as a reference to calibrate the ADXL-335 sensor.

In order to avoid an external interference for the measurements, the experimental setup was mounted in an inertial bench and the temperature in the site was controlled to be 25 °C. As the breakout board of the ADXL-335 accelerometer has two holes of 3 mm diameter, for assembling it over the standard accelerometer a support was made. The support has a cubic geometry and two holes of 3 mm were made in one of its faces to mount the MEMS accelerometer. Figures 2b and 3 show the experimental setup and procedures taken for the calibration, respectively. Also, the Arduino microcontroller was used to power the ADXL-335 accelerometer so that the measurements could be performed.

3.2 Experiment 2: 3-DOF shear building excited by an unbalanced DC motor

For the second experiment, a 3-DOF shear-building structure was mounted on the inertial bench to perform the measurements. The accelerometer that was used to compare the signals of the MEMS accelerometers was the DeltaTron Accelerometer Type 4508 Brüel and Kjær, which has a frequency range from 0.3 Hz to 8 kHz and can be used in a site with temperature from –54 to 121 °C. The acquisition system used was the USB-6251 from National Instruments and a Brüel and Kjær Model signal conditioning. In order to make the signal acquisition of the ADXL-335, -345 and the MPU-6050 accelerometers, they were connected in the Arduino Microcontroller model Mega2560. The accelerometers were mounted in the left side of the second floor of the structure,

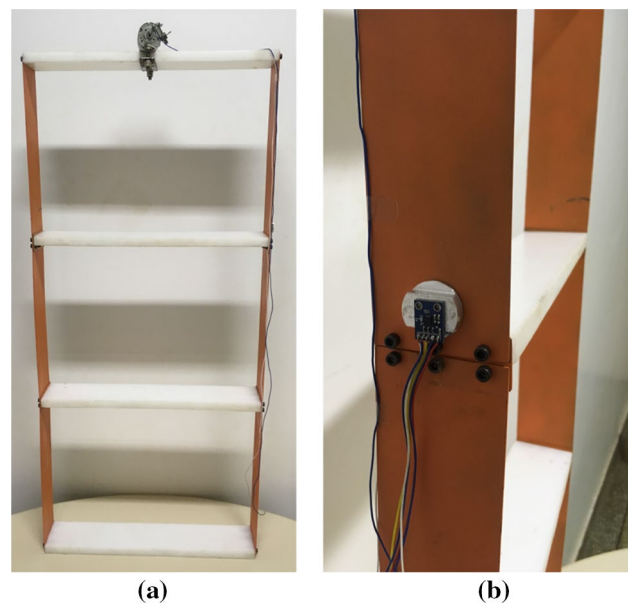
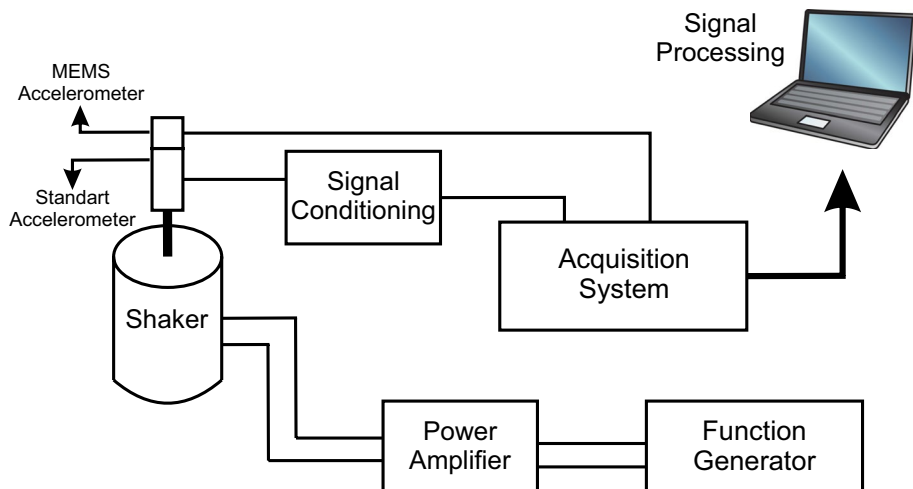


Fig. 4 **a** 3-DOF shear building in which accelerations were measured and **b** measurements' position

which was excited by an unbalanced DC motor positioned in the top floor. Figures 4a, b, 5 and 6 show the shear building considered in this paper, the position in the structure where the measurements were taken, the experimental setup of the acquisition with the MEMS and the setup for the DeltaTron, respectively.

The shear-building structure was manufactured using plates made of ASTM A-36 steel and polypropylene (Nitapro®). In total, six steel plates were used for making the laterals of the shear building which have 1.75 mm of thickness, 76.2 mm of width and 300 mm of length. For the floors of the structure, 4 polypropylene plates were used with 15

Fig. 3 Experimental procedures



mm of thickness, 76.2 mm of width and 400 mm of length. The properties of the materials used can be seen in Table 1.

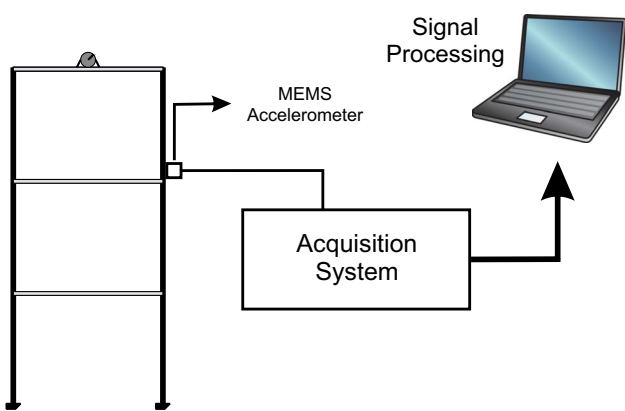


Fig. 5 Experimental setup for the MEMS accelerometer

In order to evaluate analytically, the natural frequencies of the shear building structure were discretized and modeled as a spring-mass system with 3 DOFs, where the floors were considered to be rigid. The equivalent stiffness of the structure was obtained by the material and geometrical parameters of the shear building. The calculation gave an equivalent stiffness of 983.1476 N/m for the lateral shear building. In addition, the natural frequencies were obtained through the mass and stiffness matrices applying the eigenvectors method. The results are presented in Table 2.

To excite the structure, a Mabuchi DC motor model C2162-60006 was used, in which properties can be seen in Table 3. With the purpose of unbalancing the motor, an aluminum rotor was made with holes that can be used to put masses. All the assembly of the motor and the support that mounts it in the structure have a mass of 312.15 g and an unbalance mass of 6.59 g. Figure 7 shows the voltage vs frequency curve of the motor used, which was obtained experimentally using an accelerometer and an adjustable

Fig. 6 Experimental setup for the DeltaTron accelerometer

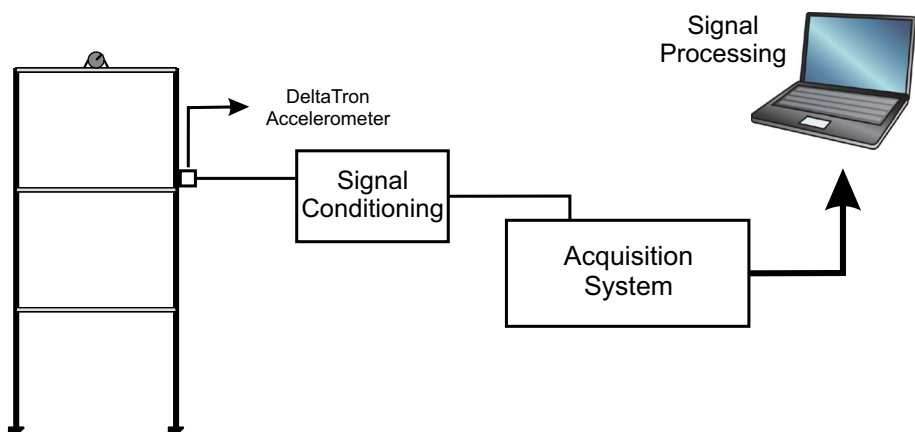


Fig. 7 Frequency curve of the motor used

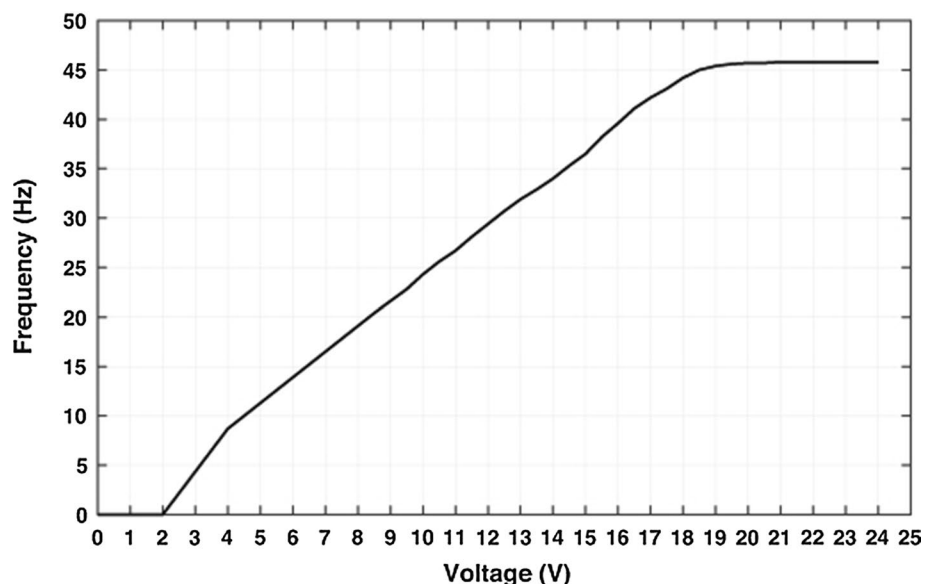


Table 1 Mechanical properties of the materials used

	ASTM A-36	Nitapro
Mass density	7850 kg/m ³	910 kg/m ³
Elastic modulus	260 GPa	1300 MPa
Ultimate tensile strength	400–450 MPa	35 MPa

Table 2 Natural frequency of the system obtained analytically

Normal modes	Value (Hz)
1° mode	4.09
2° mode	12.54
3° mode	19.32

Table 3 Properties of the motor used

Property	Value
Nominal voltage	24.0 V
Stall current	2.5 A
Stall torque	28.7 N cm
No load speed	4550.0 rpm
Start-up voltage	2.0 V
Weight	224.0 g
Shaft diameter	3.1 mm
Shaft length	85.0 mm
Motor diameter	37.0 mm
Motor length	64.0 mm

power supply, varying the voltage from 2 to 20 V with a 0.5 V increment.

4 Results and discussion

In this section, the results obtained by the calibration of the ADXL-335 and the comparison of the MEMS accelerometers with the DeltaTron sensor are presented and discussed.

4.1 Experiment 1

To perform the calibration, firstly the ADXL-335 and the standard accelerometer were connected into the Signal Analyzer, which was used to perform the amplitude measurements. In the first part of the experiment, the function generator was used to power the shaker with sinusoidal waves with amplitude of 1 g and frequency varying from 20 to 150 Hz, with 10 Hz of increment. For each value of frequency, the maximum amplitudes given by the MEMS accelerometer in the three axes were taken. The values taken correspond to the accelerometer's sensitivity in

mV/g. Also, the ADXL-335 was excited in the three axes x , y and z , with the objective of verifying whether its sensitivity was maintained with the increase in the frequency.

In the second part of the experiment, the accelerometers were excited with sinusoidal waves with amplitude of 2 g, where the frequency was also varied from 20 to 150 Hz, with a 10-Hz increment. The same procedures described in the last paragraph were performed again for this case. Moreover, the amplitudes of the three axes of the ADXL-335 were taken when subjected to excitation of amplitude 2 g.

The measurements taken with the standard accelerometer had variations of 1 ± 0.12 g. However, in order to perform a better analysis in the sensitivity of the ADXL-335 sensor, the measurements taken with it were normalized with the ones made with the standard accelerometer, i.e., the data treated in this paper are relative to 1 and 2 g, with no variation. Figure 8a–c shows the results obtained in the calibration of the MEMS sensor excited by a sinusoidal wave of amplitude 1 g and varying the frequency. Comparing them with Figure 9a–c, which show the calibration with an amplitude of 2 g, one may note that the sensitivity of the sensor maintains almost the same behavior with the increase in the amplitude. However, the figures show that the sensitivity drastically decreases with the increase in the frequency, which also raises the uncertainties in the measurements. From that, one can conclude the ADXL-335 is not advisable to use in high-frequency applications, since the uncertainties in the measurements would have a high value.

Furthermore, Tables 4, 5 and 6 show the variability of the sensitivity and the error associated with the measurements with the increase in the frequency. In the tables, the sensitivity of the sensor and the uncertainty in the measurement for each frequency band are shown. The values presented in the tables refer to the mean values of the measurement taken in each frequency, and the dispersion is the standard deviation of them. The calibration of the MEMS accelerometer showed the wider the frequency band, the measurements are being taken the lower the sensitivity and the higher the uncertainty are. One can note, for example in Table 4, that for high-frequency bands as 20–150 Hz, the error associated with the measurements has a high value of 28.89 %. However, for lower frequency as 20–30 Hz the error is 3.61 %, which, depending on the application, is a reasonable error. Hence, in low-frequency applications the ADXL-335 accelerometer can be used as a vibration sensor with reasonably precision.

4.2 Experiment 2

For the second experiment, five cases of excitation were considered for the shear building: a free oscillation with an initial displacement; a steady-state oscillation with 4, 13.12

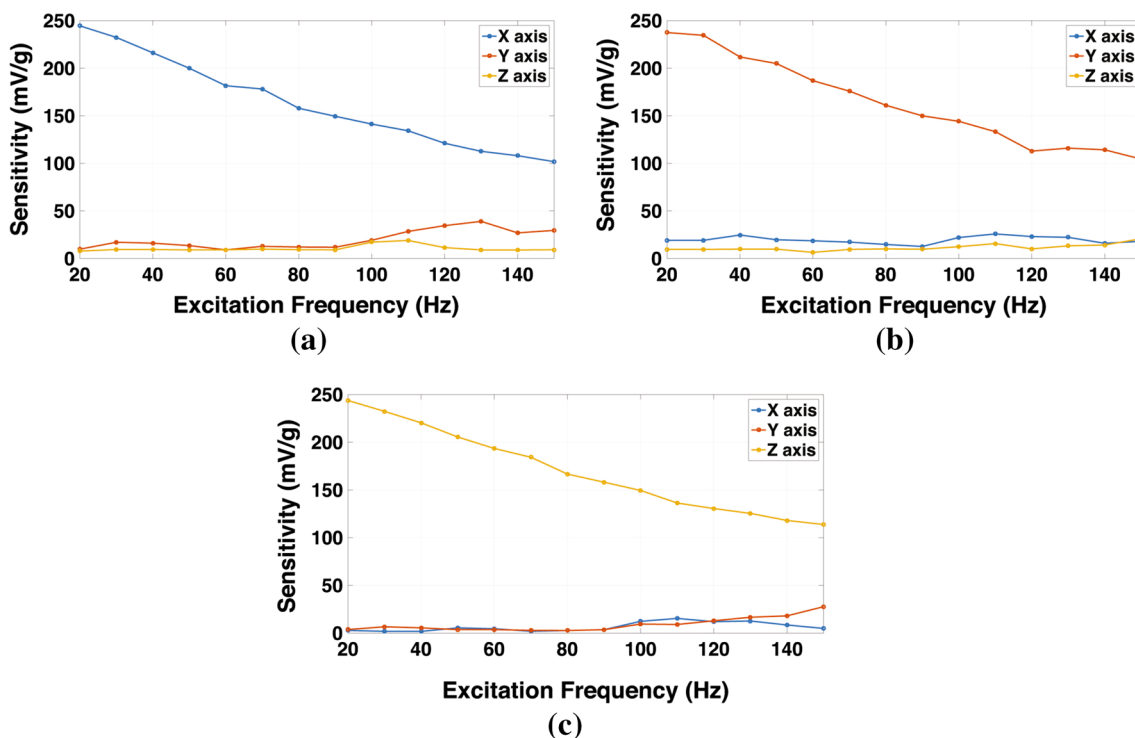


Fig. 8 Values of the sensitivity of the ADXL-335 accelerometer obtained by the excitation of sinusoidal waves of amplitude 1 g, where **a** correspond to the excitation in the *x* axis; **b** in the *y* axis; and **c** in the *z* axis

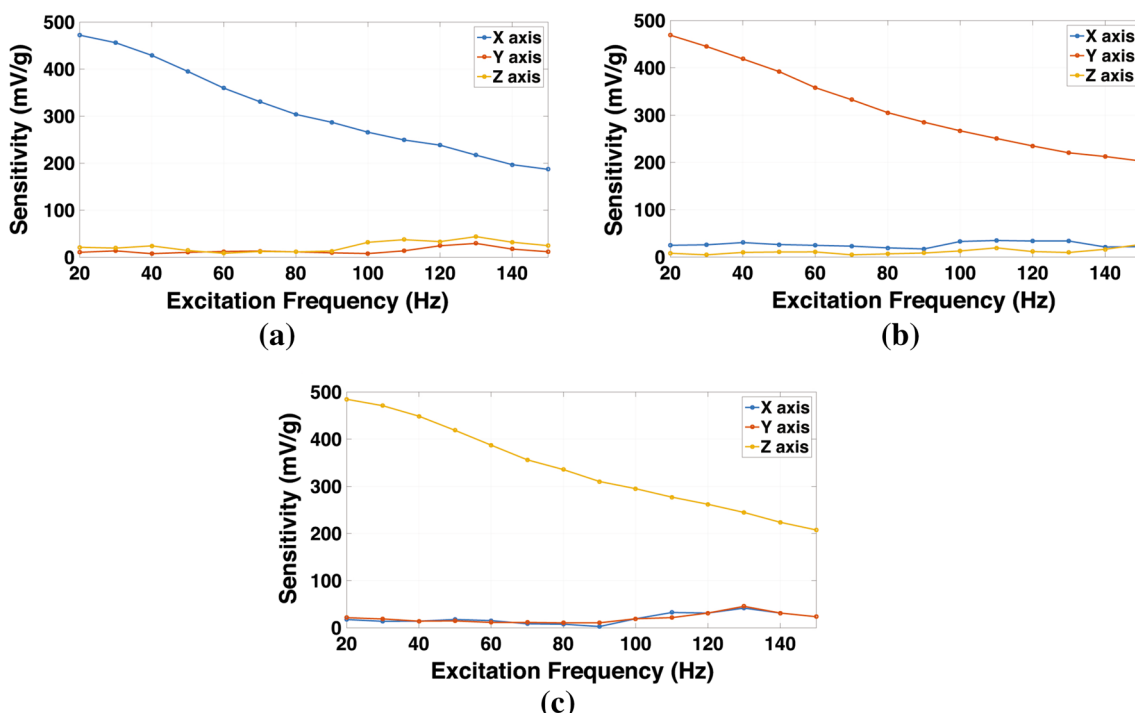


Fig. 9 Values of the sensitivity of the ADXL-335 accelerometer obtained by the excitation of sinusoidal waves of amplitude 1 g, where **a** correspond to the excitation in the *x* axis; **b** in the *y* axis; and **c** in the *z* axis

Table 4 Means and errors associated for each frequency band when the sensor is excited in the *x* axis

Frequency band (Hz)	Amplitude 1 g		Amplitude 2 g	
	Sensitivity (mV/g)	Error (%)	Sensitivity (mV/g)	Error (%)
20–30	238.47 ± 8.60	3.61	232.09 ± 5.67	2.44
20–40	231.04 ± 14.23	6.16	226.27 ± 10.84	4.79
20–50	223.28 ± 19.39	8.68	219.09 ± 16.86	7.70
20–60	214.95 ± 25.07	11.66	211.24 ± 22.84	10.82
20–70	208.83 ± 26.98	12.92	203.59 ± 27.71	13.61
20–80	201.56 ± 31.25	15.50	196.22 ± 31.95	16.29
20–90	195.06 ± 34.28	17.57	189.62 ± 34.97	18.44
20–100	189.09 ± 36.73	19.42	183.33 ± 37.77	20.60
20–110	183.61 ± 38.72	21.09	177.47 ± 40.14	22.62
20–120	177.93 ± 41.28	23.20	172.18 ± 41.93	24.36
20–130	172.50 ± 43.63	25.29	166.88 ± 43.99	26.36
20–140	167.54 ± 45.43	27.11	161.62 ± 46.19	28.58
20–150	167.55 ± 47.04	28.89	156.76 ± 47.96	30.60

Table 5 Means and errors associated for each frequency band when the sensor is excited in the *y* axis

Frequency band (Hz)	Amplitude 1 g		Amplitude 2 g	
	Sensitivity (mV/g)	Error (%)	Sensitivity (mV/g)	Error (%)
20–30	236.06 ± 2.04	0.86	228.55 ± 8.42	3.68
20–40	228.00 ± 14.03	6.15	222.17 ± 12.55	5.65
20–50	222.24 ± 16.25	7.31	215.64 ± 16.59	7.69
20–60	215.17 ± 21.15	9.83	208.34 ± 21.76	10.44
20–70	208.64 ± 24.78	11.87	201.34 ± 25.93	12.88
20–80	201.85 ± 28.89	14.31	194.39 ± 29.98	15.42
20–90	195.37 ± 32.42	16.60	187.91 ± 33.25	17.70
20–100	189.68 ± 34.79	18.34	181.87 ± 36.01	19.80
20–110	184.05 ± 37.33	20.28	176.22 ± 38.36	21.77
20–120	177.59 ± 41.39	23.31	170.88 ± 40.47	23.68
20–130	172.46 ± 43.28	25.10	165.82 ± 42.38	25.56
20–140	167.99 ± 44.47	26.47	161.24 ± 43.80	27.17
20–150	163.45 ± 45.96	28.12	156.97 ± 45.01	28.67

and 20.4 Hz of excitation; and a variable frequency of excitation from 0 to 24 Hz. In all these cases, the three MEMS and the DeltaTron accelerometer were used to measure the structure vibration so that the former could be evaluated by comparing their signals with the latter. In addition, the DeltaTron accelerometer was previously calibrated and its sensitivity was 316 mV/g.

Since our interest is to show the precision of the MEMS accelerometer in measuring frequency and amplitude of vibration, the comparison in the time and frequency domains was made, this last analysis was made using the wavelet

Table 6 Means and errors associated for each frequency band when the sensor is excited in the *z* axis

Frequency band (Hz)	Amplitude 1 g		Amplitude 2 g	
	Sensitivity (mV/g)	Error (%)	Sensitivity (mV/g)	Error (%)
20–30	238.09 ± 8.08	3.39	238.93 ± 4.85	2.03
20–40	232.19 ± 11.72	5.05	234.09 ± 9.06	3.87
20–50	225.53 ± 16.40	7.27	227.92 ± 14.39	6.31
20–60	219.13 ± 20.16	9.20	221.07 ± 19.74	8.93
20–70	213.32 ± 22.96	10.76	213.92 ± 24.87	11.63
20–80	206.66 ± 27.39	13.25	207.33 ± 28.62	13.81
20–90	200.60 ± 30.61	15.26	200.81 ± 32.29	16.08
20–100	194.92 ± 33.31	17.09	194.90 ± 35.03	17.97
20–110	189.07 ± 36.46	19.28	189.27 ± 37.52	19.82
20–120	183.75 ± 38.83	21.13	183.97 ± 39.69	21.57
20–130	178.89 ± 40.66	22.73	178.84 ± 41.81	23.38
20–140	174.22 ± 42.42	24.35	173.70 ± 44.12	25.40
20–150	169.91 ± 43.84	25.80	168.70 ± 46.32	27.46

coherence and wavelet transform. The coherence measures the correlation between two signals at a given frequency. If the signals share the same values or if they are linearly dependent at given frequencies, the magnitude of the coherence is 1; if the values presented are totally different and uncorrelated, the magnitude will be 0.

Figure 10 shows the acceleration of the free oscillation shear building measured with all the accelerometers. As one can note from the figure, the signals showed a similar character and for the MEMS accelerometers little noise is seen on the measurements. The amplitude measured by the MEMS accelerometers, however, was different from the measurement given by the DeltaTron accelerometer, as shown in Fig. 10, due to the different initial conditions given by the sensors. Also, the natural frequencies of the structure were obtained by applying the power spectrum density in the signals of the free oscillations. In Table 7, the values obtained with each accelerometer, the analytical and the finite elements method (FEM) are shown. Since the natural frequencies have low values, the MEMS accelerometers showed good results by comparing with the values shown by the DeltaTron accelerometer and the analytical as one can see from the table. In addition, the values from the FEM analysis were obtained through a CAE software.

Further, Figs. 11, 12 and 13 show the acceleration of the structure when subjected to an excitation of 4, 13.12 and 20.4 Hz, respectively. By analyzing the figures, the outcomes of the usage of the MEMS accelerometers can be seen. In addition, Fig. 14 shows the measurements of the structure vibration with a variable excitation from 0 to 24 Hz. The high peak shown in the figures corresponds to the resonance

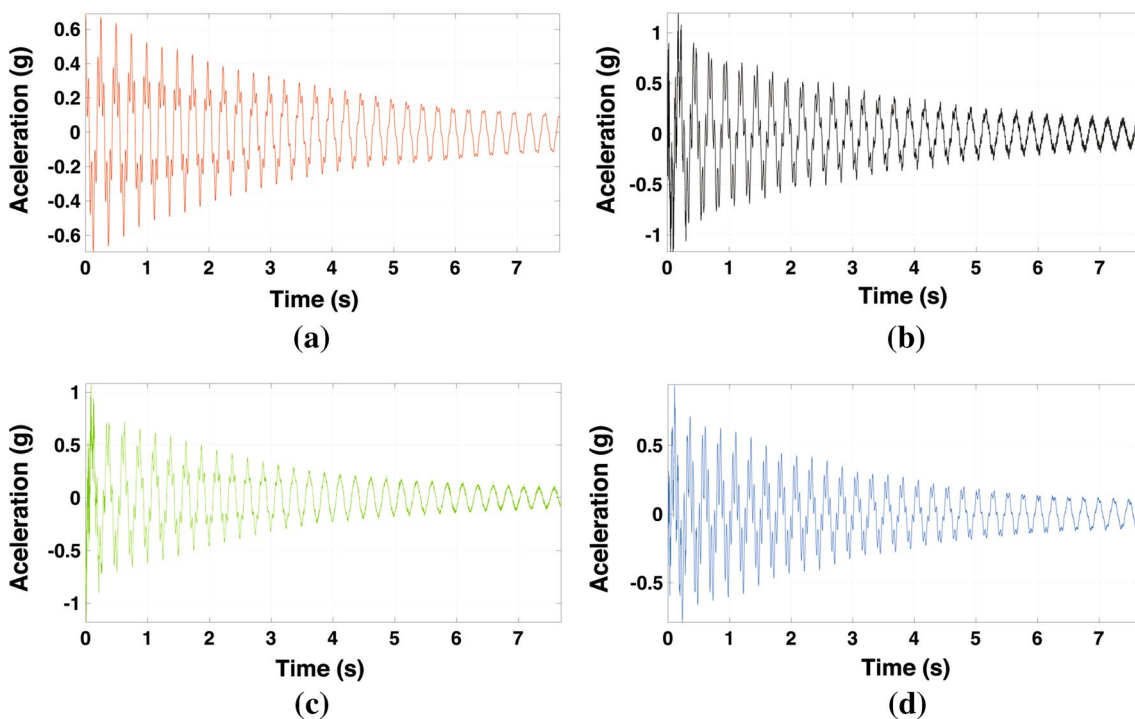


Fig. 10 Measurements of the shear-building's free vibration using: **a** DeltaTron, **b** ADXL-335, **c** ADXL-345 and **d** MPU-6050 accelerometer

Table 7 Comparison of the natural frequencies obtained analytically and experimentally

	1° mode (Hz)	2° mode (Hz)	3° mode (Hz)
Analytic	4.09	12.54	19.32
FEM analysis	4.75	14.698	24.367
DeltaTron	4.028 ± 0.000	12.94 ± 0.098	20.26 ± 0.060
MPU-5060	4.028 ± 0.000	12.94 ± 0.000	20.26 ± 0.069
ADXL-345	4.028 ± 0.000	12.94 ± 0.060	20.26 ± 0.060
ADXL-335	4.028 ± 0.000	12.94 ± 0.069	20.26 ± 0.000

of the excitation with the third natural frequency of the structure, which clearly was the most energetic one (Fig. 15).

The wavelet spectrogram was obtained with the acceleration signals for the case when the structure was excited by the motor with the frequencies of 4, 13.12 and 20.4 Hz. For such, the Wavelet Daubechies-45 was used. The scales used were from 1 to 512, 1 to 128 and 1 to 64. From the wavelet scale-frequency used, the scales that correspond to the natural frequencies of the structure were obtained, where the scale 161 corresponds to the first natural frequency, the 54 to the second and 32 to the third frequency. These scales are highlighted by the dashed green line in the spectrograms. For further reference about the wavelet transform, see [100].

The coherence between the MEMS accelerometers and the DeltaTron for the case when the structure was excited with a variation frequency was performed in the same way as

in [101, 102]. For such, the Wavelet Daubechies-45 was used again with the scales from 1 to 1024. For a better analysis of the results of the coherence, the scale-frequency curve was calculated, where the frequencies that correspond to the scales 1 and 1024, which are 500 and 0.49 Hz, were obtained, respectively. The results can be seen in Fig. 16

The graphs of the coherence showed that the measurements of the MEMS accelerometers and the DeltaTron were correlated from 5 to 40 Hz approximately, which means the MEMS sensors can be used in that frequency range with a certain precision. The ADXL-345 was the one with the measurements least correlated with the DeltaTron as one can note from Fig. 16b. The decrease in the coherence after 50 Hz shows that the MEMS accelerometers are not advisable to be used in applications with frequencies higher than this value. Also, the DeltaTron is designed to be used in high-frequency applications and it is less sensitive in low-frequency measurements, that is why the low-coherence aspect is seen in the figures from 0 to 5 Hz.

5 Concluding remarks

In this paper, the use of MEMS accelerometers to measure mechanical vibration was proposed and an evaluation of them for such usage performed. These sensors are known for their low cost and size compared to piezoelectric

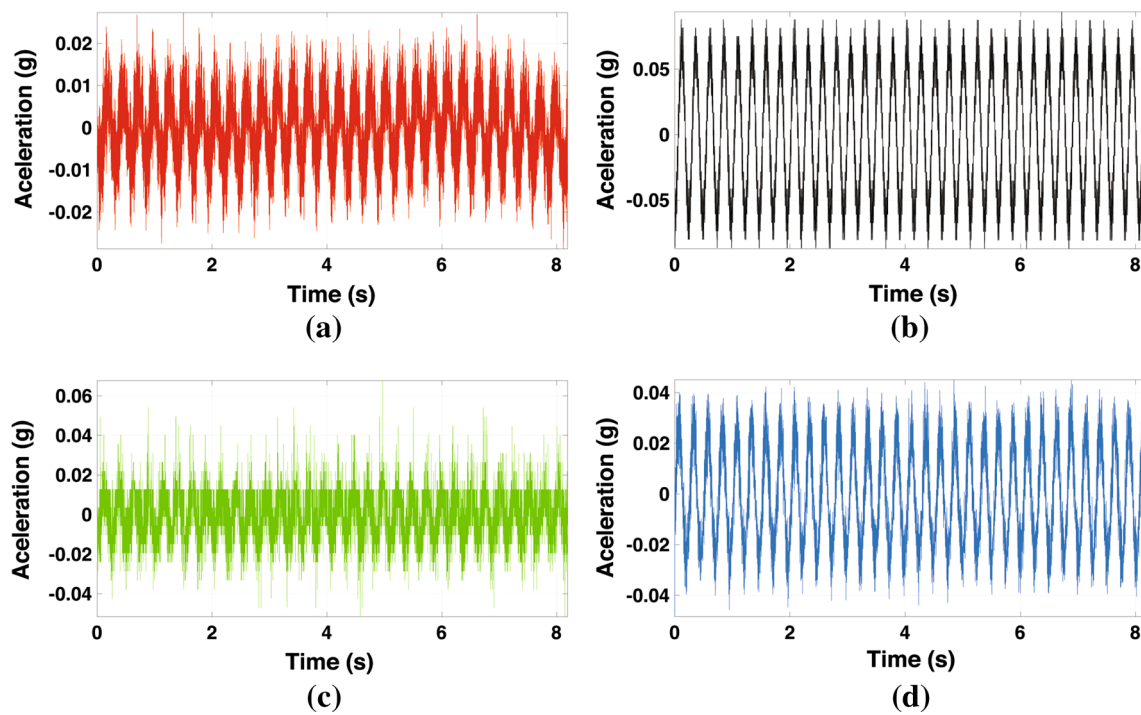


Fig. 11 Measurements of the shear-building's steady-state vibration with 4 Hz of excitation using: **a** DeltaTron, **b** ADXL-335, **c** ADXL-345 and **d** MPU-6050 accelerometer

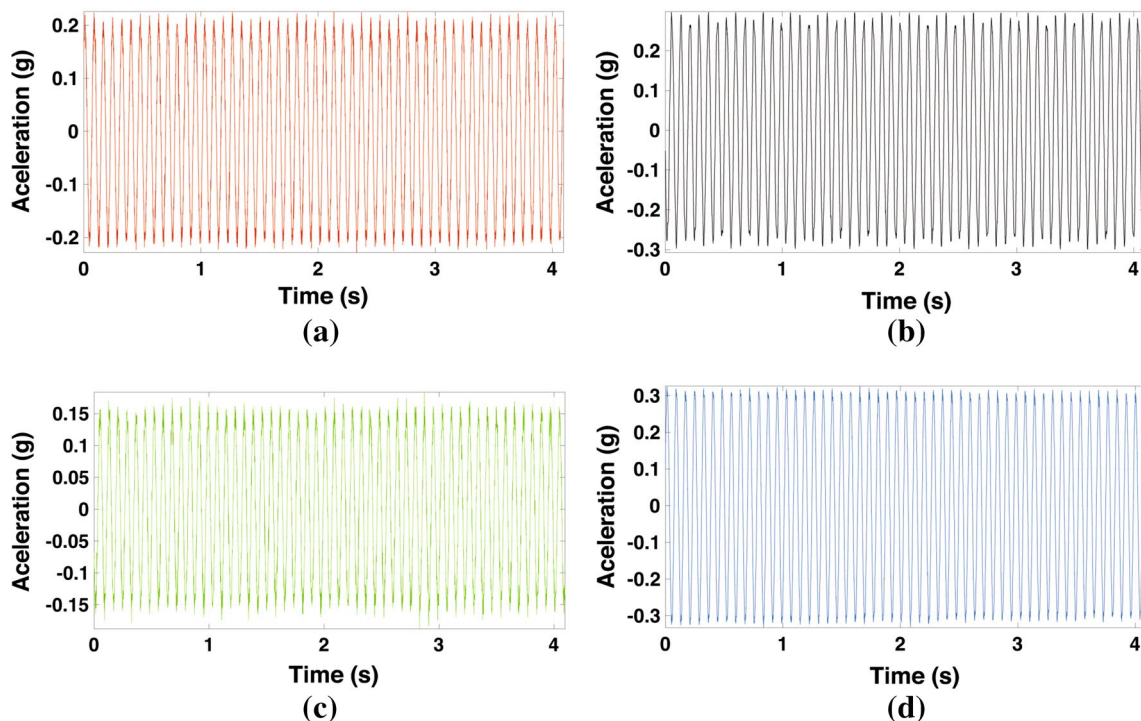


Fig. 12 Measurements of the shear-building's steady-state vibration with 13.12 Hz of excitation using: **a** DeltaTron, **b** ADXL-335, **c** ADXL-345 and **d** MPU-6050 accelerometer

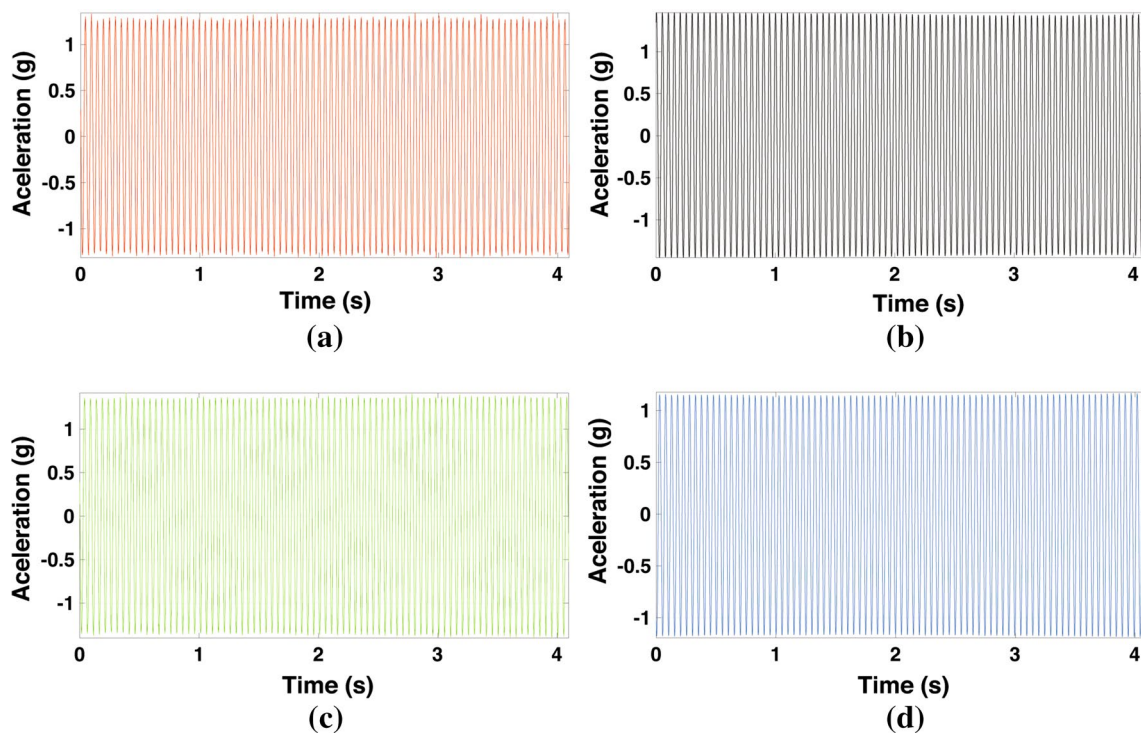


Fig. 13 Measurements of the shear-building's steady-state vibration with 20.4 Hz of excitation using: **a** DeltaTron, **b** ADXL-335, **c** ADXL-345 and **d** MPU-6050 accelerometer

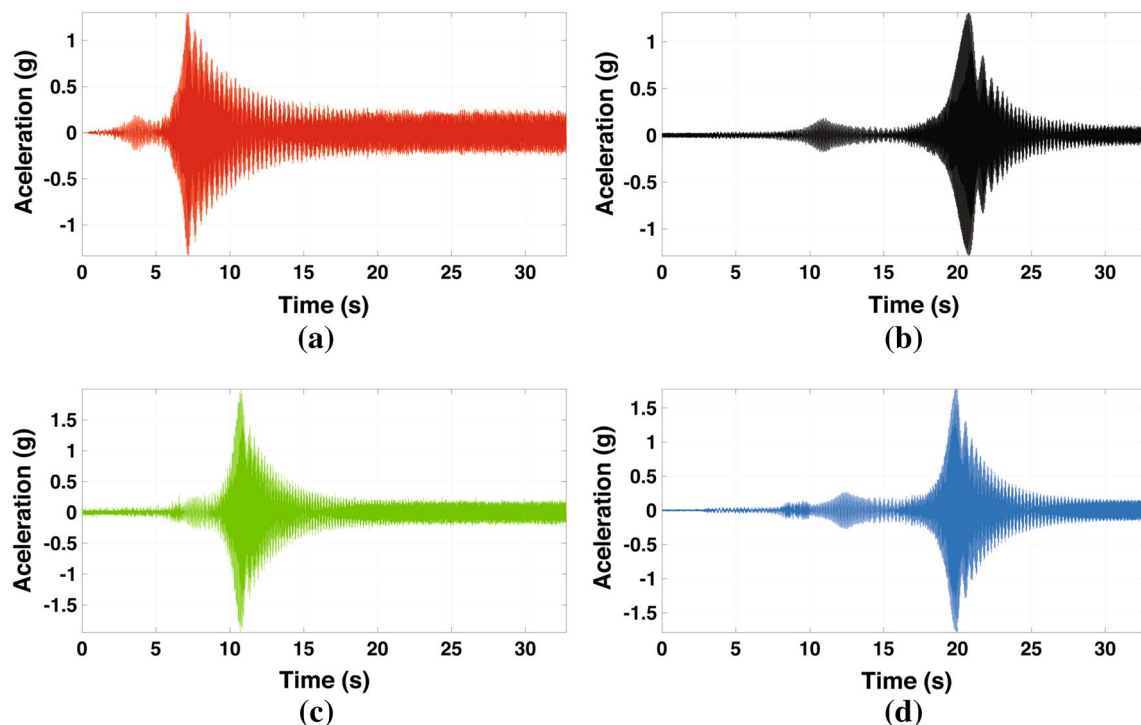


Fig. 14 Measurements of the shear-building's response to a variable excitation from 0 to 24 Hz using: **a** DeltaTron, **b** ADXL-335, **c** ADXL-345 and **d** MPU-6050 accelerometer

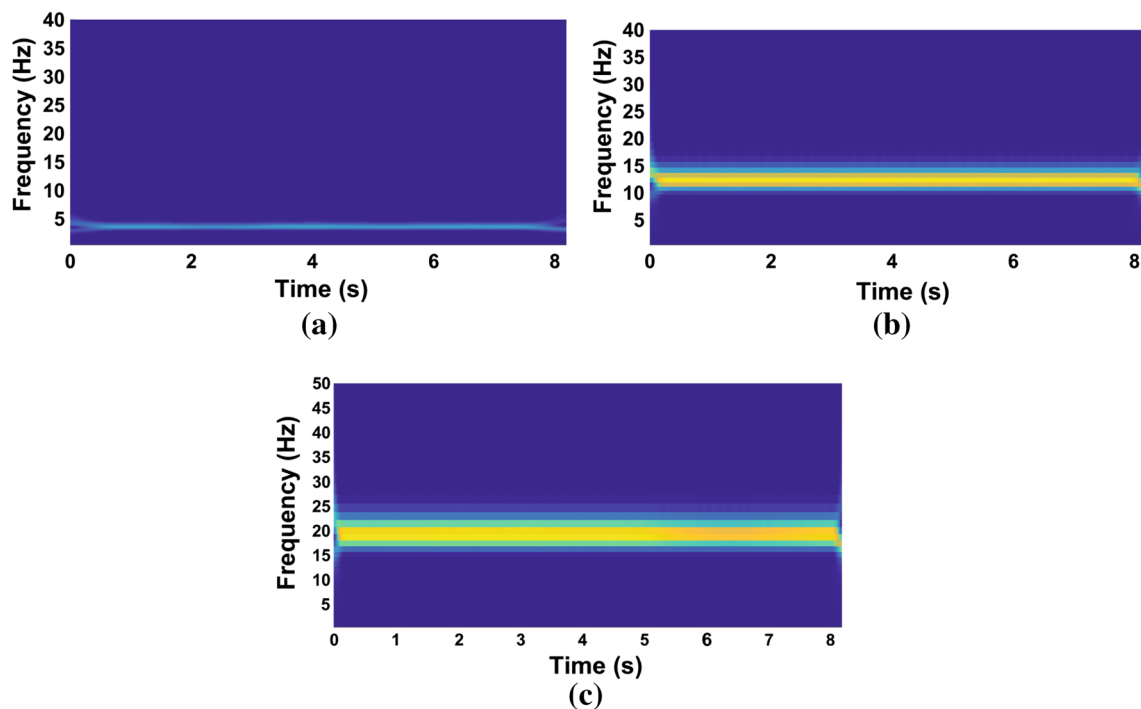


Fig. 15 Wavelet transform of the DeltaTron accelerometer when the shear building was being excited in a frequency of **a** 4, **b** 13.12 and **c** 20.4 Hz

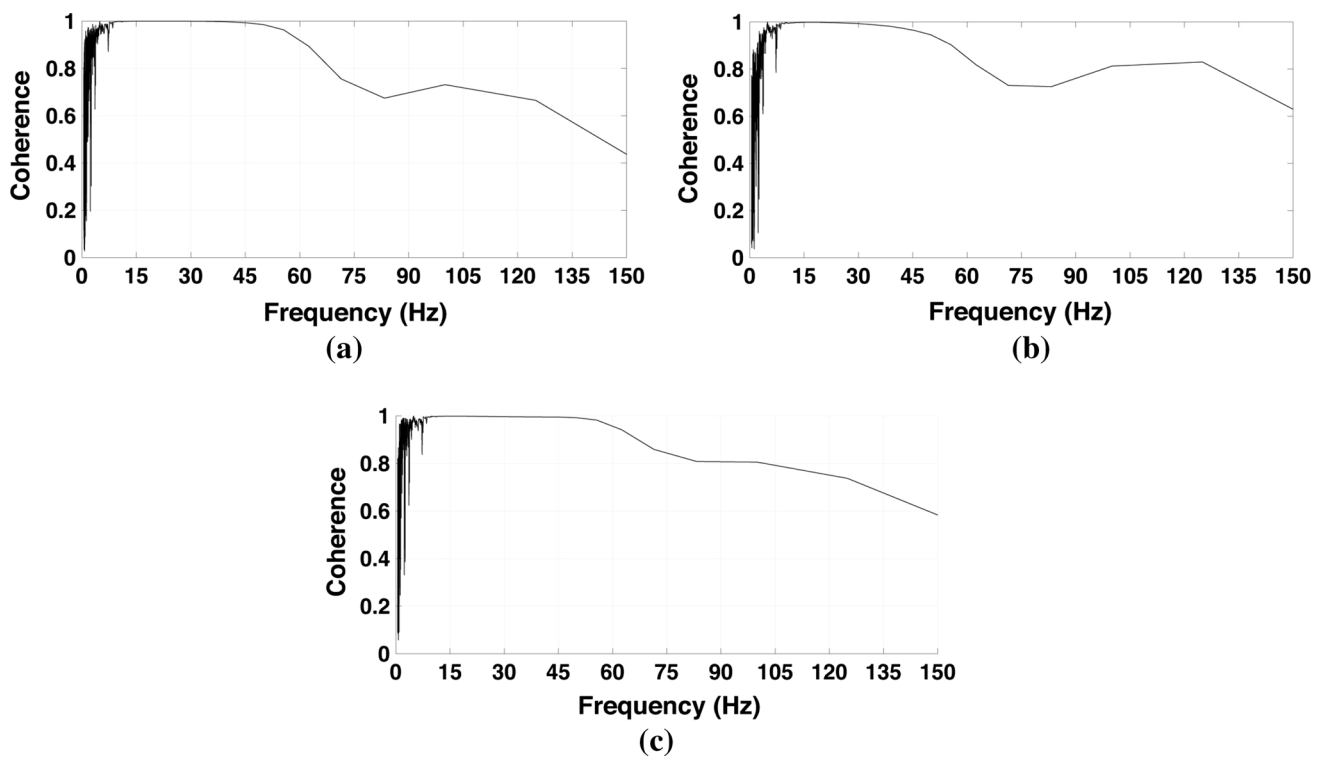


Fig. 16 Wavelet coherence of the DeltaTron with the **a** ADXL-335, **b** ADXL-345 and **c** MPU-6050 accelerometer

accelerometers. Because of these characteristics and also for their low power consumption, they are widely implemented in monitoring processes such as SHM and in energy-harvesting applications.

Two experiments were conducted in this work: the first one treated in calibrating a ADXL-335 sensor by comparing its given signals with the ones showed by a standard accelerometer when they were subjected to sinusoidal waves with different frequencies and amplitudes. The results obtained in this experiment were that the ADXL-335 has a decrease in sensitivity with the increase in the frequency of excitation, which subsequently increases the error associated in the amplitude measurements. However, in low frequencies the error presented by the measurements was little, showing that the ADXL-335 is advisable to use for measuring amplitudes in cases where there is low frequencies involved.

As for the second experiment, three MEMS accelerometers, the already calibrated ADXL-335, the MPU-605 and the ADXL-345, were evaluated by comparing the measurements given by them with a DeltaTron accelerometer in a 3-DOF shear-building structure. The signals were analyzed in time and frequency domains using the wavelet transform and the power spectrum density. In the time domain, the signals measured with the MEMS sensors presented good results by showing little noise. Also, in the frequency domain the result showed that the sensors can be used in modal analysis with a certain precision, since the measurements of the natural frequencies of the structure given by the MEMS accelerometers were very close to the one given by the DeltaTron and the analytical value. Besides, the wavelet coherence showed that the MEMS sensors can be used to measure a frequency range from 5 to 45 Hz approximately, showing that they can be used in low-frequency applications.

A similar analysis performed in this paper was performed in [84, 103]. In the former work, a three-axis waterproof analog accelerometer is presented for geoengineering applications; the results showed that the accelerometer has a good signal-to-noise ratio comparable to traditional piezoelectric accelerometers, proving that they can be used in such applications. This study showed also that the MEMS accelerometer has a more reliable measurement for frequencies below 50 Hz. On the other hand, in [103] a MEMS accelerometer is evaluated by comparing its signals with a integrated circuit piezoelectric (ICP); the accelerometers were subjected to periodic, random and impact excitation, and its given signals are compared. The results presented by this study showed that the MEMS accelerometer did well for the sinusoidal and random measurements with just little shift in phase and almost none in frequency. Although the authors claim that before the accelerometer evaluated to be used in practice, more investigation is needed. The work presented here contributes for such investigation and gives a state of the art

for the MEMS accelerometers. Also, we present an application in a well-known and important mechanical system which is the shear building and evaluated digital and analog accelerometers.

Acknowledgements The authors acknowledge the Conselho Nacional de Desenvolvimento Científico e Tecnológico (CNPq) for the support.

Appendix: A linkage diagrams

For the ADXL-335, there are five attachments in the breakout board: three of them are responsible for the acceleration data output corresponding to the three Cartesian coordinates x , y and z ; and the other two are the 5 V and the ground linkage responsible for power supply. Figure 17 shows the connection between the accelerometer and the Arduino board.

The ADXL-345 is connected to the Arduino microcontroller by means of the I2C protocol, for such the connection is made connecting the VCC, the GND, the SCA and the SCL pins of the breakout board with corresponding pins in the Arduino board. This connection can also be consulted in

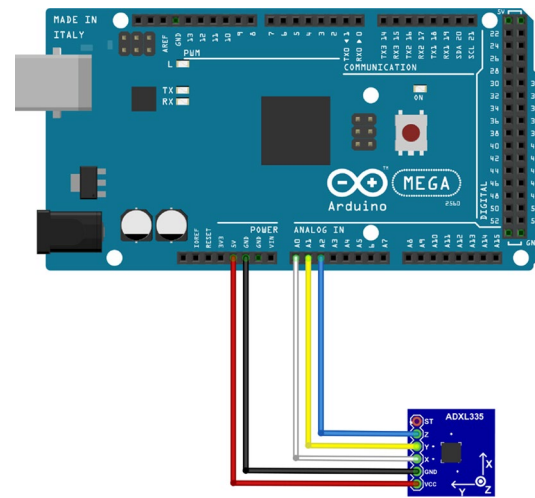


Fig. 17 Linkage diagram of the ADXL-335 sensor

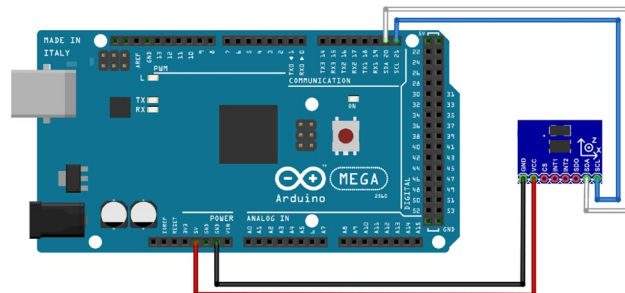


Fig. 18 Linkage diagram of the ADXL-345 sensor

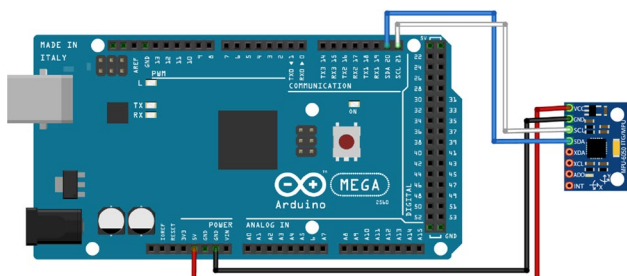


Fig. 19 Linkage diagram of the MPU-6050 sensor

Fig. 18. In addition, the connection of the MPU-6050 with the Arduino is similar to the ADXL-345, and it can be seen in Fig. 19.

References

32. Kavithaa S, Daniela RJ, Sumangalab K (2016) Design and analysis of MEMS comb drive capacitive accelerometer for SHM and seismic applications. *Measurement* 93:327–339
33. Kavitha S, Daniel RJ, Sumangala K (2013) A simple analytical design approach based on computer aided analysis of bulk micromachined piezoresistive MEMS accelerometer for concrete SHM applications. *Measurement* 46:3372–3388
34. Sheng H, Zhang T (2015) MEMS-based low-cost strap-down AHRS research. *Measurement* 59:63–72
35. Sun W et al (2013) MEMS-based rotary strapdown inertial navigation system. *Measurement* 46:2585–2596
36. Cook-Chennault KA, Thambi N, Sastry AM (2008) Powering MEMS portable devices: a review of non-regenerative and regenerative power supply systems with special emphasis on piezoelectric energy harvesting systems. *Smart Mater Struct* 17(4):043001-1–043001-33
37. Saadon S, Sidek O (2011) A review of vibration-based MEMS piezoelectric energy harvesters. *Energy Convers Manag* 52(1):500–504
38. Krüger M, Große CU, Marrón PJ (2005) Wireless structural health monitoring using MEMS. In: Key engineering materials. Trans Tech Publications, pp 625–634
39. Sohn S, Rim A, Lee I (2015) Vibration measurement of wireless sensor nodes for structural health monitoring. *Adv Sci Technol Lett* 98:18–22
40. Korkua S et al (2010) Wireless health monitoring system for vibration detection of induction motors. In: 2010 IEEE industrial and commercial power systems technical conference-conference record. IEEE, pp 1–6
41. Jaber A, Bicker R (2016) Design of a wireless sensor node for vibration monitoring of industrial machinery. *Int J Electr Comput Eng (IJECE)* 6(2):639–653
42. Albarbar A, Mekid S, Starr A, Pietruszkiewicz R (2008) Suitability of MEMS accelerometers for condition monitoring: an experimental study. *Sensors* 8:784–799
43. Son J, Niu G, Yang B, Hwang D, Kang D (2009) Development of smart sensors system for machine fault diagnosis. *Expert Syst Appl* 36:11981–11991
44. Chandrasekaran S (2015) Structural health monitoring of offshore structures using wireless sensor networking under operational and environmental variability. *Struct Health Monit* 1:42077
45. Hou L, Neil B (2011) Induction motor fault diagnosis using industrial wireless sensor networks and Dempster–Shafer classifier fusion. In: IECON 37th annual conference on IEEE industrial electronics society. IEEE, pp 2992–2997
46. Yan Y, Liu Y, Chávez JP, Zonta F, Yusupov A (2017) Proof-of-concept prototype development of the self-propelled capsule system for pipeline inspection. *Meccanica* 1–16
47. Gravina Raffaele, Alinia Parastoo, Ghasemzadeh Hassan, Fortino Giancarlo (2017) Multi-sensor fusion in body sensor networks: state-of-the-art and research challenges. *Inf Fusion* 35:68–80
48. Fortino Giancarlo, Giannantonio Roberta, Gravina Raffaele, Kuryłoski Philip, Jafari Roozbeh (2013) Enabling effective programming and flexible management of efficient body sensor network applications. *IEEE Trans Hum Mach Syst* 43(1):115–133
49. Raveendranathan Nikhil, Galzarano Stefano, Loseu Vitali, Gravina Raffaele, Giannantonio Roberta, Sgroi Marco, Jafari Roozbeh, Fortino Giancarlo (2012) From modeling to implementation of virtual sensors in body sensor networks. *IEEE Sens J* 12(3):583–593
50. Huang Q, Tang B, Deng L (2015) Development of high synchronous acquisition accuracy wireless sensor network for machine vibration monitoring. *Measurement* 66:35–44
51. Liu Z, Yuc Y, Liua G, Wangc J, Maoc X (2014) Design of a wireless measurement system based on WSNs for large bridges. *Measurement* 50:324–330
52. Bengherbia B, Zmirlia MO, Toubala A, Guessoumb A (2017) FPGA-based wireless sensor nodes for vibration monitoring system and fault diagnosis. *Measurement* 101:81–92
53. Andò B, Baglio S, Pistorio A (2014) A low cost multi-sensor approach for early warning in structural monitoring of buildings and structures. In: 2014 IEEE international instrumentation and measurement technology conference (I2MTC) proceedings. IEEE, pp 742–746
54. Son Jong-Duk, Ahn Byung-Hyun, Ha Jeong-Min, Choi Byeong-Keun (2016) An availability of MEMS-based accelerometers and current sensors in machinery fault diagnosis. *Measurement* 94:680–691
55. Jaber AA, Bicker R (2015) Real-time wavelet analysis of a vibration signal based on Arduino-UNO and LabVIEW. *Int J Mater Sci Eng* 3:66–70
56. Mane A, Rana J (2014) Vehicle collision detection and remote alarm device using Arduino. *Int J Curr Eng Technol* 4(3):2224–2228
57. Ferdoush S, Li X (2014) Wireless sensor network system design using Raspberry Pi and Arduino for environmental monitoring applications. *Procedia Comput Sci* 34:103–110
58. Naveenkumar R, Krishna P (2013) Low cost data acquisition and control using Arduino prototyping platform and LabVIEW. *Int J Sci Res (IJSR)* 2:366–369
59. Boonsawat V et al (2010) XBee wireless sensor networks for temperature monitoring. In: The second conference on application research and development (ECTI-CARD 2010), Chon Buri, Thailand
60. Varanis M et al (2016) Instrumentation for mechanical vibrations analysis in the time domain and frequency domain using the Arduino platform. *Rev Bras Ensino Física* 38(1):1301
61. Varanis M et al (2016) Instrumentation of a nonlinear pendulum using Arduino microcontroller. In: Proceedings of the XXXVII Iberian Latin-American congress on computational methods in engineering
62. Gillet D (2003) The cockpit: an effective metaphor for web-based experimentation in engineering education. *Int J Eng Educ* 19(3):389–397
63. Balogh R (2010) Educational robotic platform based on Arduino. In: Stelzer R (ed) Proceedings of the 1st international conference on robotics in education. Slovak University of Technology, Bratislava, p 119
64. Sarik J, Kymmissis I (2010) Lab kits using the Arduino prototyping platform. In: Wang Y (ed) Frontiers in education conference. IEEE, New York, p T3C-1
65. Xu R, Zhou S, Li WJ (2012) MEMS accelerometer based nonspecific-user hand gesture recognition. *IEEE Sens J* 12:1166–1173
66. Jabłoński A, Żegleń M, Staszewski W, Czop P, Barszcz (2018) How to build a vibration monitoring system on your own? *Adv Cond Monit Mach Non-Station Oper* 111–121
67. Duc TT, Le Anh T, Dinh HV (2017) Estimating modal parameters of structures using Arduino platform. In: International conference on advances in computational mechanics. Springer, Singapore, pp 1095–1104
68. Mahoney Joseph M, Nathan Rungun (2017) Mechanical vibrations modal analysis project with Arduinos. In: 2017 ASEE annual conference and exposition. American Society of Engineering Education
69. Conrad T, Schütze A (2007) A contribution for increasing the interest of high-school students for MEMS technology, engineering, and physics. *Measurement* 40:224–232

70. Lahfaoui B, Zouggar S, Mohammed B, Elhafyani ML (2017) Real time study of P&O MPPT control for small wind PMSG turbine systems using Arduino microcontroller. *Energy Procedia* 111:1000–1009
71. Yamashita RY, Silva FL, Santicioli FM, Eckert JJ, Dedini FG, Silva LC (2018) Comparison between two models of BLDC motor, simulation and data acquisition. *J Braz Soc Mech Sci Eng* 40(2):63
72. Cavalcante MA, Tavolaro CRC, Molisani E (2011) Physics with Arduino for beginners. *Rev Bras Ensino Física* 33:4503
73. Gao R, Zhang L (2004) Micromachined microsensors for manufacturing. *IEEE Instrum Meas Mag* 7:20–26
74. Badri A, Sinha J, Albarbar A (2010) A typical filter design to improve the measured signal from MEMS accelerometer. *Measurement* 43:1425–1430
75. Krzysztof T (2014) Special signals in the calibration of systems for measuring dynamic quantities. *Measurement* 49:148–152
76. Sill RD (2010) Minimizing measurement uncertainty in calibration and use of accelerometers. Endevco technical paper TP299
77. Olney D, Link B (1998) Shock and vibration measurement using variable capacitance, Endevco technical paper TP296
78. Lynch JP, Partridge A, Law KH, Kenny TW, Kiremidjian AS, Carriyer E (2003) Design of piezoresistive MEMS-based accelerometer for integration with wireless sensing unit for structural monitoring. *J Aerosp Eng* 16(3):108–114
79. Park G, Cudney HH, Inman DJ (2000) Impedance-based health monitoring of civil structural components. *J Infrastruct Syst* 6(4):153–160
80. Devices analog. ADXL335: small, low power, 3-axis ± 3 g accelerometer. ADXL335 Data Sheet Rev B (2010)
81. Kavitha S, Daniel R, Joseph Sumangala K (2016) Design and analysis of MEMS comb drive capacitive accelerometer for SHM and seismic applications. *Measurement* 93:327–339
82. Gonenil IE, Celik-Butler Z, Donald P (2011) Surface micromachined MEMS accelerometer on flexible polyimide substrate. *IEEE Sens J* 11:2318–2326
83. Zheng Q, Zhang Y, Lei Y, Song J, Xu Y (2010) Haircell-inspired capacitive accelerometer with both high sensitivity and broad dynamic range. In: IEEE sensors conference, China
84. Bhattacharya S et al (2012) Economic MEMS based 3-axis water proof accelerometer for dynamic geo-engineering applications. *Soil Dyn Earthq Eng* 36:111–118
85. Swathy L, Abraham L (2014) Analysis of vibration and acoustic sensors for machine health monitoring and its wireless implementation for low cost space applications. In: 2014 First international conference on computational systems and communications (ICCS). IEEE, pp 80–85
86. Hoffman K, Varuso R, Fratta D (2006) The use of low-cost MEMS accelerometers in near-surface travel-time tomography. In: Proceedings of the GeoCongress 2006 conference, Atlanta, GA
87. Jing B, Leon K (2013) Demonstration of self-powered accelerometer using piezoelectric micro-power generator. In: Research and development (SCOReD). IEEE, pp 560–563
88. Lisowski M (2016) Structural damage detection using wireless passive sensing platform based on RFID technology. *Struct Control Health Monit* 23:1135–1146
89. Patil SS (2015) Sensor based bridge condition monitoring system using GSM. *Int J Emerg Trends Sci Technol* 2:2152–2156
90. Kale A, Jagtap S (2015) Detection of stator, rotor and bearing faults of induction motor using lab view. *Asian J Converg Technol* 1:1146–2350
91. Gorlatova M (2015) Movers and shakers: Kinetic energy harvesting for the internet of things. *IEEE J Sel Areas Commun* 33:1624–1639
92. Weddell A et al (2012) Vibration-powered sensing system for engine condition monitoring. In: IET conference on wireless sensor systems, p 22
93. Zhu D et al (2009) A self powered tag for wireless structure health monitoring in aeronautical applications. In: PowerMEMS, pp 201–204
94. Raj V et al (2013) Induction motor fault detection and diagnosis by vibration analysis using MEMS accelerometer. In: 2013 International conference on emerging trends in communication, control, signal processing and computing applications (C2SPCA). IEEE
95. Zheng Y et al (2014) Machine tool vibration fault monitoring system based on internet of things. In: China conference on wireless sensor networks, Springer, Berlin, pp 533–547
96. Toma D et al (2014) Experimental validation and modeling of plucked piezoelectric for underwater energy harvesting system. In: 20th IMEKO TC4 International symposium and 18th international workshop on ADC modelling and testing: research on electric and electronic measurement for the economic upturn: proceedings, pp 45–49
97. Liao Y et al (2016) Angular velocity-based structural damage detection. In: SPIE smart structures and materials+ nondestructive evaluation and health monitoring, International Society for Optics and Photonics, p 98031N
98. Galdino E, Cury A (2017) Development of low-cost wireless accelerometer for structural dynamic monitoring. *Rev Interdiscip Pesqui Eng RIPE* 2:10–19
99. Xiaoyan H, Kuang KSC (2016) Structural motion monitoring systems using 9-axis sensing modules. In: The 2016 structure congress (structures 16)
100. Yan R, Gao RX, Chen X (2014) Wavelets for fault diagnosis of rotary machines: a review with applications. *Signal Process* 96:1–15
101. Torrence Christopher, Compo Gilbert P (1998) A practical guide to wavelet analysis. *Bull Am Meteorol Soc* 79(1):61–78
102. Kopal J et al (2014) Complex continuous wavelet coherence for EEG microstates detection in insight and calm meditation. *Conscious Cognit* 30:13–23
103. Albarbar A, Badri A, Sinha J, Starr A (2009) Performance evaluation of MEMS accelerometers. *Measurement* 42:790–795